ANALYSIS OF SHELL-TYPE STRUCTURES SUBJECTED TO TIME-DEPENDENT MECHANICAL AND THERMAL LOADING

A SEMI-ANNUAL STATUS REPORT
SUBMITTED TO
NASA-LEWIS RESEARCH CENTER
CLEVELAND, OHIO

By

G.J. Simitses
R.L. Carlson
R. Riff

School of Aerospace Engineering
Georgia Institute of Technology
Atlanta, Georgia

April 1987

(NASA GRANT: NAG 3-534)

INTRODUCTION

The objective of the present research is to develop a general mathematical model and solution methodologies for analyzing structural response of thin, metallic shell-type structures under large transient, cyclic or static thermomechanical loads. Among the system responses, which are associated with these load conditions, are thermal buckling, creep buckling and ratchetting. Thus, geometric as well as material-type nonlinearities (of high order) can be anticipated and must be considered in the development of the mathematical model. Furthermore, this must also be accommodated in the solution procedures.

SUMMARY OF PROGRESS

The progress update has been elaborated upon in an interim scientific report submitted to the sponsor during the summer of 1986. A second report, describing the developed finite element, the computer code, and several

applications to cylindrical and spherical shell configurations, is being prepared. It is expected that this second scientific report will be submitted to the sponsor during the summer of 1987.

A complete true ab-inito rate theory of kinematics and kinetics for continuum and curved thin structures, without any restriction on the magnitude of the strains or the deformation, was formulated. The time dependence and large strain behavior are incorporated through the introduction of the time rates of the metric and curvature in two coordinate systems; a fixed (spatial) one and a convected (material) coordinate system. The relations between the time derivative and the covariant derivative (gradient) have been developed for curved space and motion, so that the velocity components supply the connection between the equations of motion and the time rate of change of the metric and curvature tensors.

The metric tensor (time rate of change) in the convected material coordinate system is linearly decomposed into elastic and plastic parts. In this formulation, a yield function is assumed, which is dependent on the rate of change of stress, metric, temperature, and a set of internal variables. Moreover, a hypoelastic law was chosen to describe the thermoelastic part of the deformation.

A time and temperature dependent viscoplastic model was formulated in this convected material system to account for finite strains and rotations. The history and temperature dependence were incorporated through the introduction of internal variables. The choice of these variables, as well as their evolution, was motivated by phenomenological thermodynamic considerations.

The nonisothermal elastic-viscoplastic deformation process was described completely by "thermodynamic state" equations. Most investigators (in the area of viscoplasticity) employ plastic strains as state variables. Our study shows that, in general, use of plastic strains as state variables may lead to inconsistencies with regard to thermodynamic considerations. Furthermore, the approach and formulation employed by all previous investigators lead to the condition that all plastic work is completely dissipated. This, however, is in contradiction with experimental evidence, from which it emerges that part of the plastic work is used for producing residual stresses in the lattice, which, when phenomenologically considered, causes hardening.

Both limitations are not present in our formulation, because of the inclusion of the "thermodynamic state" equations.

The obtained complete rate field equations consist of the principles of the rate of the virtual power and the rate of conservation of energy, of the constitutive relations, and of boundary and initial conditions. These formulations provide a sound basis for the formulation of the adopted finite element solution procedures.

One of the most challenging aspects of finite strain formulations is to locate analytical solutions with which to compare the proposed formulation. Typically, as a first problem, a large strain uniaxial test case was analyzed. The case considered examines the rate-dependent plastic response of a bar to a deformation history that includes segments of loading, unloading, and reloading, each occurring at varying strain and temperature rates. Moreover, it was shown that the proposed formulation generates no strain energy under a pure rigid body rotation. These are surely important demonstrations but they only represent a partial test because the principal stretch directions remain constant. Finally, a problem which was discussed by Nagtegaal and de Jong, and others too, as a problem which demonstrates limitations of the consitutive models in many strain formulations, is the Couette flow problem. This problem is solved as a third example. The results of these test problems show that:

- The formulation can accommodate very large strains and rotations.
- The formulation does not display the oscillatory behavior in the streses of the Couette flow problem.
- The model incorporates the simplifications associated with rate-insensitive elastic response without losing the ability to model rate temperature dependent yield strength and plasticity.

The problem of buckling of shallow arches under transient thermomechanical load was investigated next.

The quasi-linear nature of the principle of the rate of virtual power suggests the adoption of an incremental approach to numerical integration with respect to time. The availability of the field formulation provides assurance of the completeness of the incremental equations and allows the use of any convenient procedure for spatial integration over the domain V. In the present instance, the choice has been made in favor of a simple first

order expansion in time for the construction of incremental solutions from the results of finite element spatial integration of the governing equations.

The procedure employed permits the rates of the field formulation to be interpreted as increments in the numerical solution. This is particularly convenient for the construction of incremental boundary condition histories.

Even under the condition of static external loads and slowly growing creep effects, the presence of snap-through buckling makes the inertia effects significant. In dynamic analyses, the applied body forces include inertia forces. Assuming that the mass of the body considered is preserved, the mass matrix can be evaluated prior to the time integration using the initial configuration.

Finite element solution of any boundary-value problem involves the solution of the equilibrium equations (global) together with the constitutive equations (local). Both sets of equations are solved sinultaneously in a step by step manner. The incremental form of the global and local equations can be achieved by taking the integration over the incremental time step $\Delta t=t_{j+1}-t_j$. The rectangular rule has been applied to execute the resulting time integration.

Clearly, the numerical solution involves iteration. A simplified version of the Riks-Wempner constant-arc-length method has been utilized. This iteration procedure which is a generalization of the displacement control method also allows to trace the nonlinear response beyond bifurcation points. In contrast to the conventional Newton-Raphson techniques, the iteration of the method takes place in the velocity and load rate space. The load step of the first solution in each increment is limited by controlling the length ds of the tangent. Either the length is kept constant in each step or it is adapted to the characteristics of the solution. In each step the triangular-sized stiffness matrix has to be checked for negative diagonal terms, indicating that a critical point is reached.

The analysis was performed with the aid of 24 paralinear isoparametric elements. The paralinear isoparametric element is intended for the analysis of oriented structures where the geometry is such that the thickness is small compared to other dimensions. The characteristics of the element are defined by the geometry and interpolation functions, which are linear in the thickness direction and parabolic in the longitudinal direction. Consequently,

the element allows for shear strain energy since normals to a mid-surface before deformation remain straight, but not necessarily normal to the mid-surface after deformation.

The developed solution scheme is capable of predicting response which includes pre- and post-buckling with thermal creep and plastic effects. The solution procedure was demonstrated through several examples which include both creep and snap-through behavior.

The last set of problems which are under investigation consists of creep or thermal buckling with plastic effects of shells of revolution.

To develop geometrically nonlinear, doubly-curved finite shell elements the basic equations of nonlinear shell theories have to be transferred into the finite element model. As these equations are in general written in tensor notation, their implementation into the finite element matrix formulation requires considerable effort.

The nonlinear element matrices were derived directly from the incrementally formulated nonlinear shell equations, by using a tensor-oriented procedure. A modified version of the classical thin shell theory based on the Kirchoff-Love hypotheses, capable of large strains and rotations, is presently employed. For this formulation, we are using five "natural" degrees of freedom per mid-surface shell node: three incremental velocities and two rates of rotations about the material coordinates α^1 and α^2.

This element was introduced to the solution procedure described earlier. Few examples of creep and thermal buckling of a cylindrical panel and spherical cap are currently under investigation.

In connection with the progress to date, two papers were published in the AIAA Journal and one in the "NASA-U. of Akron Sponsored Meeting" Proceedings. Copies of these papers have been mailed to the sponsor. Moreover, two papers appeared in the Proceedings of the 28th AIAA/ASME/ASCE/AHS SDM Conference. Copies of these two papers are attached herewith.

FUTURE TASKS

With regard to additional future tasks, one must include the development of a finite element accommodating the more general shell theory formulations (A,B, & C), and the incorporation of this into a code. Moreover, three-dimensional effects, especially those associated with normal stresses, will

be incorporated, either through modification of the developed shell theory or through local-global finite element procedures in which the local part will be based on three-dimensional analysis.

Finally, another important extension is to replace the material constitution (initially homogeneous and isotropic-metal) by a more general one that allows the analysis of layered fiber-reinforced composites.

A COLLECTION OF TECHNICAL PAPERS PART 1

Structures and Materials
(Sessions #1-3, 6-9, 12-15, 18-21, 24, 27-29, 32-35)

AIAA/ASME/ASCE/AHS
28TH STRUCTURES, STRUCTURAL DYNAMICS AND MATERIALS CONFERENCE
April 6-8, 1987/Monterey, California

87-0804

SOLUTION METHODS FOR ONE-DIMENSIONAL VISCOELASTIC PROBLEMS

by

John M. Stubstad* and George J. Simitses**
School of Engineering Science and Mechanics
Georgia Institute of Technology
Atlanta, Georgia 30332

Abstract

A recently developed differential methodology for solution of one-dimensional nonlinear viscoelastic problems is presented. Using the example of an eccentrically loaded cantilever beam-column, the results from the differential formulation are compared to results generated using a previously published integral solution technique. It is shown that the results obtained from these distinct methodologies exhibit a surprising high degree of correlation with one another. A discussion of the various factors affecting the numerical accuracy and rate of convergence of these two procedures is also included. Finally, the influences of some "higher order" effects, such as straining along the centroidal axis are discussed.

I. Introduction

A number of methods are available to solve viscoelastic problems in which the behavior of the material may be adequately characterized by a linear viscoelastic operator and where the deformation of the body is sufficiently small to allow the use of a linear kinematic formulation [1,2]. Commonly, integral transform methods, separation of variables, series expansions or other such techniques provide methodologies wherein exact closed form solutions may be derived. When exact solutions cannot be obtained, approximate techniques, such as one proposed by Schapery [3], may provide an alternate approach.

The inclusion of nonlinear effects in the analysis significantly reduces the mathematical tractability of the problem. These nonlinear influences can be induced by geometric factors resulting from the magnitude of the deformation or from gross rotation of cross sections. Alternatively, nonlinearities in the material response may need be included to provide an accurate model for material behavior.

Independent of whether these nonlinearities are produced by geometric or material effects, they invariably result in an overall formulation governed by nonlinear equations. Thus, the solution methods mentioned above, applicable to linear problems, cannot be employed. As such, approximate solution methods have been developed and are routinely employed to analyze such problems [4].

One of these methods is to idealize the problem is such a manner so as to generate inherent simplifications to the governing relations. A classical example of this technique was the utilization of an ideal "I" cross sectional geometry in early column creep buckling studies [5]. With this approximation, the equations governing equilibrium of the column were reduced to much simpler forms involving the "average" stresses in the flanges of the ideal beam-column.

Another approach used extensively was to restrict considerations to only certain types of time dependent material behavior [6]. In some cases, this involved retaining only secondary creep behavior in the material model. Alternatively, and especially when "power law" type constitutve laws were used, the constants or exponents of the law were restricted to special values for which closed form solution was possible [7]. In a few cases, this simplification of the material model, as well as the aforementioned geometric simplification technique, were employed simultaneously to enable solution. A survey of most of these methods has been provided by Hoff [8].

An exact numerical solution technique for geometrically nonlinear viscoelastic problems has been presented by Rogers and Lee [9]. A recent paper by the authors [10] provides a method for bounding the solution for such problems. In both of these techniques, the solution to the problem is formulated in terms of an integral equation which is nonlinear with respect to both time and space. From this, solutions may then be readily obtained using relatively standard numerical techniques. Generally, both the exact and bounding technique can be employed for problems wherein the response of the material may be adequately characterized using a linear viscoelastic model, but where the resulting time dependent deformation of the body warrants the use of a nonlinear kinematic formulation.

*Currently with the Aerospace Corporati .
El Segundo, California; Member ASME.
**Professor of Aerospace Engineering.
Associate Fellow AIAA; Member ASME.

Since the integral solution technique can be applied only when the response of the material either is or may be reasonably approximated as being linear, problems involving nonlinear viscoelastic material behavior cannot be addressed using these methods. Unfortunately, many materials, and especially the elevated temperature behavior of most metals, require such nonlinear characterizations. Consequently, an alternate solution procedure for one-dimensional problems involving nonlinear kinematic and nonlinear material effects has been developed. This method, hereinafter referred to as the differential formulation, is based on the direct solution of the nonlinear differential equations of equilibrium.

Similar to the integral method, the overall procedure is predicated on the assumption of a quasistatic response. This assumption effectively "decouples" the temporal and spatial dependence of the problem in such a manner so as to allow the general solution to be treated as the combination of the solutions to a nonlinear "boundary value" problem and a nonlinear "initial value" problem. The first of these, the equations characterizing the time dependent states of quasistatic equilibrium, are solved through the use of a Newton type method [11]. In contrast, the "initial value" problem, resulting from the nonlinear constitutive law, governs the manner by which the body progresses from one state of quasistatic equilibrium to the succeeding one. Numerical solutions for this part of the problem are generated using a fourth order Runge-Kutta method. Using this technique, problems involving the nonlinear thermoviscoelastic behavior of thin structural members have recently been examined [12].

In addition to presenting the differential formulation technique, a comparison of results obtained through the use of the integral and differential formulations is provided. The problem of an eccentrically loaded viscoelastic cantilever beam-column is employed as the vehicle through which the comparison is performed. Because of the inherent limitation of the integral technique, this comparison is restricted to the consideration of a linear viscoelastic material. The specific case considered is that of the three parameter viscoelastic solid which has been examined in a number of studies [10,13,14]. The results obtained from these two distinct methods of solution exhibit a surprisingly high degree of correlation with one another thereby establishing a high level of confidence in the validity of the methods. Finally, the differential formulation is employed to examine the influences of some of the "higher order" effects for the class of problems under consideration.

II. Integral Formulation

Since the integral solution is available in literature [9,10], only a brief outline of its development is presented herein. The solution is based on the assumption that the beam-column is thin and composed of a linearly viscoelastic material. Its geomerty in the deformed configuration is illustrated in Fig. 1. Note that the eccentric load is assumed to be applied quasistatically and its direction does not vary with time.

Reference line extensional strains are assumed to be negligibly small. Thus the coordinate s' is employed to specify position in both the initial and deformed configurations. A nondimensional coordinate, s, is defined by dividing s' by the length of the beam, L. Assuming a linear distribution of the strains through the depth, bending thus occuring within a Bernoulli-Euler context, results in a moment-curvature relationship given by

$$\kappa(s',t) = \left(\frac{1}{I}\right)\int_{-\infty}^{t} J(t-\tau)\left[\frac{\partial M(s',\tau)}{\partial \tau}\right] d\tau \qquad (1)$$

where $\kappa(s',t)$ denotes the curvature and $M(s',\tau)$ the bending moment at location s'. I is the moment of inertia of the beam and $J(t)$ the creep compliance of the material. For the eccentric load, $R(t)$, the moment at position s' is given by

$$M(s',\tau) = R(\tau)[\delta(\tau) + a\cos\alpha(\tau) - y(s',\tau)] \qquad (2)$$

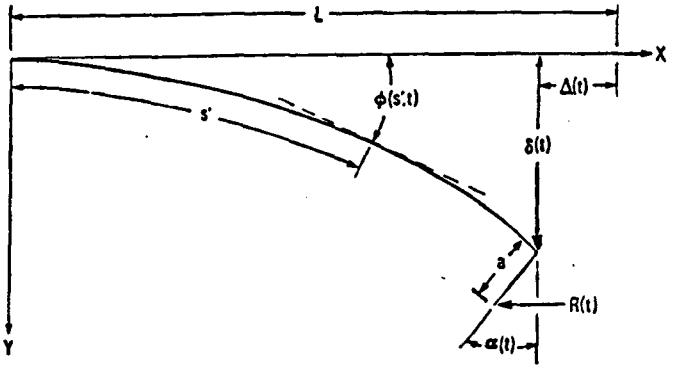

Figure 1. Beam-Column Geometry for Integral Formulation

From kinematic considerations, it is noted that

$$\kappa(s',t) = \frac{\partial \phi(s',t)}{\partial s'}$$
$$\frac{\partial x(s',t)}{\partial s'} = \cos\phi(s',t) \qquad (3)$$
$$\frac{\partial y(s',t)}{\partial s'} = \sin\phi(s',t)$$

The boundary conditions for the problem are

$$\phi(0,t) = 0$$
$$M(L,t) = aR(t)\cos\phi(L,t) \qquad (4)$$

where $\alpha(t) = \phi(L,t)$ for a "rigid" extension.

Substituting Eqns. (2) and (3) into Eqn. (1) followed by differentiation with respect to s yields the governing differential equation. Using the methodology detailed in [9], it can be

shown that, for quiescent initial conditions, the solution for this equation is given by

$$\phi(s,t) = \left(\frac{L^2}{I}\right)\left[J(0)R(t)\Theta(s,t) + \int_0^t J'(t-\tau)R(\tau)\Theta(s,\tau)\,d\tau\right] \tag{5}$$

where

$$\Theta(s,t) = \left(\frac{sa}{L}\right)\cos\phi(1,t) + \int_0^1 g(s,u)\sin\phi(s,t)\,du \tag{6}$$

and

$$\begin{aligned} g(s,u) &= u, \quad 0 \le u \le s \\ &= s, \quad s \le u \le 1 \end{aligned} \tag{7}$$

and where the prime, (′), in Eqn. (5) denotes differentiation with respect to the argument of the function.

Note that Eqn. (5) represents a time convolution of a nonlinear Fredholm type integral equation, Eqn. (6). Numerical solutions for this set of equations are accomplished using Picard's method of successive substitutions [15]. The spatial integrals are approximated using Newton-Coates formulae; a fixed step trapezoidal rule is used for the time convolution.

III. Differential Formulation

Similar to the integral formulation, the differential formulation for this problem is based on the assumption that bending of the beam occurs in accordance with the Euler-Bernoulli hypotheses. The functions $u(s,t)$ and $w(s,t)$ are employed to denote, respectively, the axial and transverse deflection of points on the centroidal axis. From this, the extensional strain along the centroidal axis, ϵ_o, is approximately given by

$$\epsilon_o \approx \frac{\partial u}{\partial s} + \frac{1}{2}\left(\frac{\partial w}{\partial s}\right)^2 \tag{8}$$

Note that the term $\frac{1}{2}(\frac{\partial u}{\partial s})^2$ has been neglected as small in comparison to $\frac{\partial u}{\partial s}$. If, in addition, both the strain at the centroidal axis and $\frac{\partial u}{\partial s}$ are small in comparison to 1 then it is relatively simple to show that

$$\frac{\partial \phi}{\partial s} \approx \frac{\partial w}{\partial s}\frac{\partial^2 u}{\partial s^2} - \frac{\partial^2 w}{\partial s^2}. \tag{9}$$

Thus, for a linear variation of strain through the cross section, this yields

$$\epsilon_{11} = \epsilon_o + \eta\frac{\partial \phi}{\partial s} \tag{10}$$

Employing the Principle of Virtual Work followed by integrating by parts and then manipulating algebraically eventually yields the equilibrium equations

$$N = -F\left(1 + \frac{\partial u}{\partial s} + \frac{\partial \phi}{\partial s}\left(a\cos\phi(L) + w(s) - w(L)\right)\right) \tag{11a}$$

and

$$M = F\left(a\cos\phi(L) + w(s) - w(L)\right) \tag{11b}$$

where N and M, the force and moment resultants, respectively, are defined as

$$N = \int_A \sigma_{11}\,dA \quad \text{and} \quad M = \int_A \eta\sigma_{11}\,dA. \tag{12a,b}$$

Based upon an additive decomposition for total strain, ϵ_t, such that $\epsilon_t = \epsilon_e + \epsilon_c$ where ϵ_e and ϵ_c represent the elastic and creep strain components, respectively, yields, after substitution into Eqns. (11) and (12),

$$EA\epsilon_o = -F\left(1 + \frac{\partial u}{\partial s} + \frac{\partial \phi}{\partial s}\left(a\cos\phi(L) + w(s) - w(L)\right)\right) - N_c \tag{13a}$$

and

$$EI\frac{\partial \phi}{\partial s} = F\left(a\cos\phi(L) + w(s) - w(L)\right) + M_c \tag{13b}$$

where A represents the area of the cross section. I denotes its moment of inertia and the "pseudo-resultants" N_c and M_c are defined by

$$N_c = \int_A E\epsilon_c\,dA \quad \text{and} \quad M_c = \int_A \eta E\epsilon_c\,dA \tag{14a,b}$$

Numerical solutions for Eqns. (14) are computed using a modified Newton type method suggested by Thurston [15]. To illustrate this method consider a nonlinear differential term of the form $du^m dw^n$ where du and dw are differentials of the functions u and w and m and n represent integer exponents. Assuming that close trial solutions $\tilde{w}$ and $\tilde{u}$ are available which differ from the exact solution by the small quantities Δw and Δu so that $u = \tilde{u} + \Delta u$ and $w = \tilde{w} + \Delta w$, then

$$\begin{aligned} du^m\,dw^n = {} & d\tilde{u}^m\,d\tilde{w}^n + m\,d\tilde{u}^{m-1}\,d\tilde{w}^n\,d(\Delta u) \\ & + n\,d\tilde{u}^m\,d\tilde{w}^{n-1}\,d(\Delta w) + f(\tilde{u},\tilde{w})O(\Delta u, \Delta w) \end{aligned} \tag{15}$$

where $f(\,)$ denotes a nonlinear function of $\tilde{u}$ and $\tilde{w}$ and O indicates terms of order $\Delta u \Delta w$ and higher. If the trial solution is indeed close to the true solution, then the corrections, Δu and Δw, will be small. Consequently, the quadratic and higher order terms in the corrections will be negligible in comparison to the linear terms and therefore may be neglected. Thus, under these conditions, the right-hand side of Eqn. (15) may be closely approximated by the linearized form consisting of just the first three terms on the right-hand side.

With this type of procedure, the original nonlinear differential equation is incrementally approximated by a linearized form. Employing standard finite-difference formulae, the linearized form is then converted into a system of algebraic equations where the unknowns are the corrections to the trial solution at the nodes of the finite difference mesh. These relations are solved for these corrections, the trial solution is adjusted and the process repeated until convergence is obtained.

Numerical solution of Eqns. (13) also requires evaluation of the "pseudo-resultants" N_c and M_c at each point of the finite-difference mesh. This is accomplished by evaluating the accumulated creep strain at select number of points across the cross section and then using a three point Newton-Coates quadrature formula repetitively to approximate the area integral. Evaluation of the accumulated creep strain at each of these points is accomplished through the use of a fourth order Runge-Kutta integration routine to integrate the constitutive law expressed in a differential format.

IV. Example Problem

The specific example considered is that of a 12 in. long beam-column. For simplicity, a square cross section of dimension 0.5 in. has been assumed. It is also assumed that the beam-column is fabricated from a material which can be modeled as a three parameter viscoelastic solid. The creep compliance for this model. illustrated in Fig. 2, is given by

$$J(t)/J(0) = 1 + [E_2/E_1]e^{-t/\tau_o} \qquad (16)$$

where $\tau_o = \eta_1/E_1$. For these computations, the numerical values for the parameters have been selected so that $\tau_o = 1$. Thus, integer values for time equal multiples of the time constant of the material.

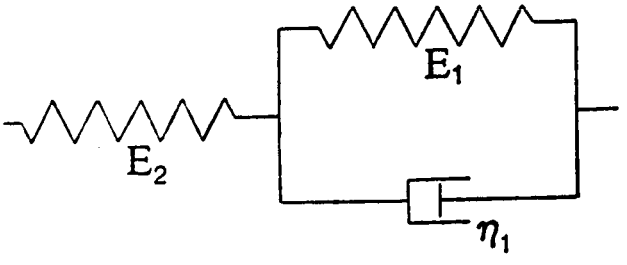

Figure 2. Ideal Three Element "Limited" Creep Model.

A five point grid in the transverse direction is used for computation of the "pseudo-resultants" in the differential formulation. The points are equidistantly spaced with the first and last located at the extreme fibers and the central point positioned on the centroidal axis.

Since the solutions of both the differential and integral formulations are only satisfied at a discrete number of points over the length of the beam-column, the first question that must be addressed is how sensitive the results are to the number of points used in the approximation. Table 1 provides a comparison of the variation of the results from the differential formulation for the initial elastic deflection of the beam-column as the number of approximating points is doubled from 10 to 20 and then doubled again to 40 for an eccentricity ratio of 0.05 and an applied load of $P/P_e = 0.75$. The Euler load, P_e, here is based on a perfect geometry and use of the instantaneous compliance of the material, $J(0)$. Table 2 provides a similar comparison for the same loading and eccentricity ratio but for the integral formulation.

Table 1. Differential Elastic Solution Versus Number of Nodes for $P/P_e = 0.75$ and $a/L = 0.05$

Transverse Deflection for Various Numbers of Elements (in)

	Number of Elements		
$s = s'/L$	40	20	% Diff
0.0	0.000000	0.000000	
0.1	0.024673	0.024705	0.130
0.2	0.098189	0.098307	0.120
0.3	0.219074	0.219332	0.118
0.4	0.384931	0.385376	0.116
0.5	0.592512	0.593187	0.114
0.6	0.837815	0.838755	0.112
0.7	1.116191	1.117426	0.111
0.8	1.422456	1.424007	0.109
0.9	1.750997	1.752879	0.107
1.0	2.095877	2.098098	0.106
$s = s'/L$	40	10	% Diff
0.0	0.000000	0.000000	
0.1	0.024673	0.024809	0.551
0.2	0.098189	0.098763	0.585
0.3	0.219074	0.220289	0.555
0.4	0.384931	0.387110	0.566
0.5	0.592512	0.595755	0.547
0.6	0.837815	0.842435	0.551
0.7	1.116191	1.122177	0.536
0.8	1.422456	1.430090	0.537
0.9	1.750997	1.760165	0.524
1.0	2.095877	2.106817	0.522

(% differences are with respect to 40 element solution)

From these two Tables it can be seen that there is very little change in the computed transverse deflection as the number of approximating points is increased. In both cases, the initial elastic solution of the ten element model is within 1.0 % of the 40 element model results. Additionally, the relative magnitude of the errors between the 10 and 40 element models of the differential formulation are virtually identical to those exhibited by the integral solution methodology. Although not specifically indicated on these Tables, it should also be noted that the angles of rotation are not always small. For example, at this load and eccentricity, the initial elastic end rotation of the beam-column exceeds 17 deg. Of course, smaller rotations are exhibited at the lower loads and lower eccentricities.

Table 2. Integral Elastic Solution Versus Number of Nodes for $P/P_e = 0.75$ and $a/L = 0.05$

Transverse Deflection for Various Numbers of Elements (in)

	Number of Elements		
$s = s'/L$	40	20	% Diff
0.0	0.000000	0.000000	
0.1	0.024616	0.024652	0.146
0.2	0.097967	0.098125	0.161
0.3	0.218586	0.218890	0.139
0.4	0.384079	0.384691	0.159
0.5	0.591200	0.592089	0.150
0.6	0.835951	0.837267	0.157
0.7	1.113686	1.115374	0.152
0.8	1.419227	1.421422	0.155
0.9	1.746972	1.749594	0.150
1.0	2.091003	2.094171	0.152
$s = s'/L$	40	10	% Diff
0.0	0.000000	0.000000	
0.1	0.024616	0.024781	0.670
0.2	0.097967	0.098753	0.802
0.3	0.218586	0.220123	0.703
0.4	0.384079	0.386547	0.643
0.5	0.591200	0.595443	0.718
0.6	0.835951	0.841727	0.691
0.7	1.113686	1.120936	0.651
0.8	1.419227	1.429034	0.691
0.9	1.746972	1.758422	0.655
1.0	2.091003	2.105685	0.702

(% differences are with respect to 40 element solution)

Therefore, it is concluded that both formulations exhibit the same low level of sensitivity to the number of elements used in the analysis. Concurrently, these results also indicate that a 10 element model can be used with either method without generating significant errors in the analysis. It should be noted that all of the differential formulation results presented above are based on the use of an exact expression for evaluating the angle of rotation.

A direct comparison between the results generated by the two formulations is provided in Tables 3 and 4. Again, the comparison is based on the 0.50 eccentricity ratio which inherently produces larger angles of rotation. The angle of rotation of the cross section, determined from the integral technique, are also provided.

Table 3 is based on the use of an exact expression for evaluation of $\sin\phi$ in the solution of the differential methodology. The "approximate" $\sin\phi$ results, provided in Table 4, on the other hand, are based on use of the common approximation $\sin\phi \approx -\partial w/\partial s$, to calculate the angle of rotation. Note that, other than this particular change, these two differential formulations are, otherwise, completely identical. Both include the influences of axial as well as transverse deflection on the behavior of the beam-column. The influence of deleting the axial deformation on the accuracy of the predicted results is discussed later.

Table 3. Integral and Differential ($\frac{\partial}{\partial t}$) Elastic Solutions for Various Loads $a/L = 0.05$

Transverse Deflection from Various Solutions (in)

$s = s'/L$	Integral	Exact $\sin\phi$ $\partial/\partial t$	% Diff	Angle (deg)
		for $P/P_e = 0.25$		
0.0	0.000000	0.000000		0.00
0.1	0.002615	0.002616	0.04	0.25
0.2	0.010450	0.010448	−0.02	0.50
0.3	0.023444	0.023445	0.00	0.74
0.4	0.041520	0.041531	0.03	0.98
0.5	0.064590	0.064589	0.00	1.22
0.6	0.092475	0.092483	0.01	1.44
0.7	0.125010	0.125031	0.02	1.66
0.8	0.162039	0.162044	0.00	1.87
0.9	0.203256	0.203279	0.01	2.07
1.0	0.248513	0.248497	−0.01	2.25
		for $P/P_e = 0.50$		
0.0	0.000000	0.000000		0.00
0.1	0.008283	0.008285	0.02	0.79
0.2	0.033056	0.033044	−0.04	1.57
0.3	0.073940	0.073948	0.01	2.33
0.4	0.130441	0.130516	0.06	3.07
0.5	0.202009	0.201999	0.00	3.76
0.6	0.287513	0.287559	0.02	4.40
0.7	0.385945	0.386070	0.03	5.01
0.8	0.496357	0.496382	0.01	5.52
0.9	0.616919	0.617049	0.02	6.01
1.0	0.746772	0.746670	−0.01	6.38
		for $P/P_e = 0.75$		
0.0	0.000000	0.000000		0.00
0.1	0.024781	0.024809	0.11	2.37
0.2	0.098753	0.098763	0.01	4.68
0.3	0.220123	0.220289	0.08	6.91
0.4	0.386547	0.387110	0.15	9.03
0.5	0.595443	0.595755	0.05	10.97
0.6	0.841727	0.842435	0.08	12.68
0.7	1.120936	1.122177	0.11	14.23
0.8	1.429034	1.430090	0.07	15.41
0.9	1.758422	1.760165	0.10	16.44
1.0	2.105685	2.106817	0.05	17.04

(% differences are with respect to integral solution)
(comparisons based on results from 10 element models)

As the data of these Tables indicate, there are no significant differences in predicted transverse deflections. Even for an end rotation angle of 17 deg, the differences between the various results is well below that required in engineering computations. It should be noted that this high level of correlation continues to exist for even greater angles of rotation. The reason why this high correlation exists is that, under compressive loading, the derivative of the axial displacement is negative. Since, the square of the slope of the transverse deflection is always positive, these algebraically combine so that the sum is lower in magnitude than either of the individual terms. This serves to reduce the magnitude of the centroidal axis strain. Because the differ-

Table 4. Integral and Differential ($\frac{\partial}{\partial t}$) Elastic Solutions for Various Loads $a/L = 0.05$

$s = s'/L$	Integral	Approx. $\sin\phi$ $\partial/\partial t$	% Diff	Angle (deg)
		Transverse Deflection from Various Solutions (in)		
		for $P/P_e = 0.25$		
0.0	0.000000	0.000000		0.00
0.1	0.002615	0.002616	0.00	0.25
0.2	0.010450	0.010448	−0.02	0.50
0.3	0.023444	0.023445	0.00	0.74
0.4	0.041520	0.041531	0.03	0.98
0.5	0.064590	0.064589	0.00	1.22
0.6	0.092475	0.092483	0.01	1.44
0.7	0.125010	0.125031	0.02	1.66
0.8	0.162039	0.162044	0.00	1.87
0.9	0.203256	0.203279	0.01	2.07
1.0	0.248513	0.248497	−0.01	2.25
		for $P/P_e = 0.50$		
0.0	0.000000	0.000000		0.00
0.1	0.008283	0.008286	0.04	0.79
0.2	0.033056	0.033044	−0.04	1.57
0.3	0.073940	0.073949	0.01	2.33
0.4	0.130441	0.130516	0.06	3.07
0.5	0.202009	0.202000	0.00	3.76
0.6	0.287513	0.287560	0.02	4.40
0.7	0.385945	0.386071	0.03	5.01
0.8	0.496357	0.496383	0.01	5.52
0.9	0.616919	0.617050	0.02	6.01
1.0	0.746772	0.746672	−0.01	6.38
		for $P/P_e = 0.75$		
0.0	0.000000	0.000000		0.00
0.1	0.024781	0.024810	0.12	2.37
0.2	0.098753	0.098767	0.01	4.68
0.3	0.220123	0.220299	0.08	6.91
0.4	0.386547	0.387128	0.15	9.03
0.5	0.595443	0.595782	0.06	10.97
0.6	0.841727	0.842473	0.09	12.68
0.7	1.120936	1.122228	0.12	14.23
0.8	1.429034	1.430155	0.08	15.41
0.9	1.758422	1.760244	0.10	16.44
1.0	2.105685	2.106911	0.06	17.04

(% differences are with respect to integral solution)
(comparisons based on results from 10 element models)

ence between the exact and approximate expressions for $\sin\phi$ is related to the $\sqrt{1+2\epsilon_o}$ in the denominator of the exact expression, reducing the magnitude of the centroidal strain inherently improves the accuracy of the approximation.

This influence is best illustrated by the data of Table 5. Here, the integral solution is compared to an approximate solution for which the effect of the centroidal axis strain terms has been suppressed. This was accomplished by first eliminating all the $(\partial w/\partial s)^2$ terms from the governing equations. The EA modulus-area product was then artificially increased through multiplication by a factor of 1000. This second change reduces the magnitude of the axial deflection by approximately the same factor.

The net result of these changes is to create a differential model where the centroidal axis effectively is inextensional. While it might be anticipated that this would improve the correlation between the differential and integral results, such is not the case. When the angle of rotation is very small, as those which result from a low level of loading and a small eccentricity, all the formulations provide virtually identical predictions. However, as the angle of rotation increases, as those which occur at the higher loadings and the greater load eccentricity, the modified differential formulation predictions begin to diverge from those of the other two. The difference between the predicted results is most notable for the highest load and largest load eccentricity example.

Table 5. Integral and Modified Differential ($\frac{\partial}{\partial t}$) Elastic Solutions for Various Loads $a/L = 0.05$

$s = s'/L$	Integral	Modified (w/o ϵ_o) $\partial/\partial t$	% Diff	Angle (deg)
		Transverse Deflection from Various Solutions (in)		
		for $P/P_e = 0.25$		
0.0	0.000000	0.000000		0.00
0.1	0.002615	0.002616	0.00	0.25
0.2	0.010450	0.010446	−0.04	0.50
0.3	0.023444	0.023444	0.00	0.74
0.4	0.041520	0.041527	0.02	0.98
0.5	0.064590	0.064586	−0.01	1.22
0.6	0.092475	0.092478	0.00	1.44
0.7	0.125010	0.125030	0.02	1.66
0.8	0.162039	0.162043	0.00	1.87
0.9	0.203256	0.203287	0.02	2.07
1.0	0.248513	0.248508	0.00	2.25
		for $P/P_e = 0.50$		
0.0	0.000000	0.000000		0.00
0.1	0.008283	0.008294	0.13	0.79
0.2	0.033056	0.033073	0.05	1.57
0.3	0.073940	0.074032	0.12	2.33
0.4	0.130441	0.130665	0.17	3.07
0.5	0.202009	0.202274	0.13	3.76
0.6	0.287513	0.287975	0.16	4.40
0.7	0.385945	0.386711	0.20	5.01
0.8	0.496357	0.497264	0.18	5.52
0.9	0.616919	0.618270	0.22	6.01
1.0	0.746772	0.748235	0.20	6.38
		for $P/P_e = 0.75$		
0.0	0.000000	0.000000		0.00
0.1	0.024781	0.025543	3.07	2.37
0.2	0.098753	0.101698	2.98	4.68
0.3	0.220123	0.227057	3.15	6.91
0.4	0.386547	0.399299	3.30	9.03
0.5	0.595443	0.615237	3.32	10.97
0.6	0.841727	0.870876	3.46	12.68
0.7	1.120936	1.161483	3.62	14.23
0.8	1.429034	1.481683	3.68	15.41
0.9	1.758422	1.825548	3.82	16.44
1.0	2.105685	2.186716	3.85	17.04

(% differences are with respect to integral solution)
(comparisons based on results from 10 element models)

This behavior results from the way the end of the beam-column deflects. In the modified model, the end of the beam-column basically moves only in the vertical direction (see Fig. 1). The standard model, however, allows the end to move both vertically and horizontally. Thus, for a given vertical deflection, the leftward movement predicted by the standard model increases the angle of rotation. This reduces the moment by reducing the moment arm. Thus, to support a given load, the standard formulation beam-column model need not deflect as much as the modified model must.

Comparisons of the viscoelastic predictions provided by the integral and the exact differential are provided in Table 6. A comparison with the approximate $\sin\phi$ differential solution is not included because the differences between the exact and approximate results again are so small as to be negligible. These computations are based on the use of an ideal three element "limited" material model illustrated in Fig. 2.

As demonstrated by the data of this Table, the high correlation between the elastic solutions provided by the integral and differential solution methods carries over directly into the viscoelastic analysis.

The final item meriting discussion is the length of the time increment used in each of the formulations. Unlike the prior results, some differences do exist between the maximum allowable time step increments for the integral and differential formulations. Additionally, the allowable time step increment for the integral formulation exhibits a higher dependence on the actual angle of rotation than does the differential formulation.

In general, a relatively small time step increment must be used with the integral solution methodology. For example, the results presented above are based on the use of a 0.01 time step. As the length of this time step is increased, the accuracy of the solution decreases and tends to underpredict the deflection. This convergence "from below" is not surprising since the convolution integral is approximated as the sum of a finite number of terms.

In contrast, much larger time step increments can be used with the differential formulation. This is principally attributed to the high accuracy provided by the Runge-Kutta integration routine. Most of the results provided above were developed using a 0.10 time step. Additionally, the allowable length for this time step increment tended to be rather insensitive to the angle of rotation. The allowable time step for the integral formulation, on the other hand, exhibited a high level of sensitivity to the angle of rotation. Larger angles of rotation required significantly shorter time steps for accurate results to be obtained.

These factors combine in a rather interesting manner with regard to which method of analysis is computationally more efficient. Typically, for the analysis of short periods of viscoelastic deformation the integral solution method was two to three times faster than the differential method. This is attributed to

Table 6. Integral and Differential Viscoelastic Solutions for Three Time Constants $P/P_e = 0.50$, and $a/L = 0.05$

	Transverse Deflection (in)			
$s = s'/L$	Integral	Exact $\sin\phi$ $\partial/\partial t$	% Diff	Angle (deg)
		at time = 0.0		
0.0	0.000000	0.000000		0.00
0.1	0.008283	0.008285	0.02	0.79
0.2	0.033056	0.033044	−0.04	1.57
0.3	0.073940	0.073948	0.01	2.33
0.4	0.130441	0.130516	0.06	3.07
0.5	0.202009	0.201999	0.02	3.76
0.6	0.287513	0.287559	0.02	4.40
0.7	0.385945	0.386070	0.03	5.01
0.8	0.496357	0.496382	0.01	5.52
0.9	0.616919	0.617049	0.02	6.01
1.0	0.746772	0.746670	−0.01	6.38
		at time = 1.0		
0.0	0.000000	0.000000		0.00
0.1	0.015083	0.015089	0.04	1.44
0.2	0.060151	0.060128	−0.04	2.86
0.3	0.134319	0.134344	0.02	4.22
0.4	0.236430	0.236612	0.08	5.54
0.5	0.365200	0.365193	0.00	6.76
0.6	0.518035	0.518161	0.02	7.86
0.7	0.692634	0.692946	0.05	8.87
0.8	0.886869	0.886967	0.01	9.70
0.9	1.096666	1.097006	0.03	10.44
1.0	1.320154	1.320004	−0.01	10.95
		at time = 2.0		
0.0	0.000000	0.000000		0.00
0.1	0.019127	0.019138	0.06	1.83
0.2	0.076254	0.076232	−0.03	3.62
0.3	0.170149	0.170202	0.03	5.34
0.4	0.299200	0.299484	0.09	7.00
0.5	0.461621	0.461664	0.01	8.52
0.6	0.653844	0.654093	0.04	9.85
0.7	0.872716	0.873246	0.06	11.13
0.8	1.115343	1.115622	0.03	12.12
0.9	1.376227	1.376871	0.05	12.99
1.0	1.652861	1.652902	0.00	13.55

(% differences are with respect to integral solution)
(comparisons based on results from 10 element models)

two factors. The first is the comparitively slow Runge-Kutta integration procedure used in the differential formulation. For a short period of viscoelastic deformation, the calculation of the convolution integral of the integral formulation, requiring simple summation of a limited number of terms, can be performed much more rapidly.

The second factor is that the fixed point iteration scheme of the integral formulation, although requiring more iterations than the Newton method, is also performed more rapidly since it is simply an algebraic operation. The Newton method, in contrast, requires inversion of the matrix premultiplying the vector of trial function corrections and then numerical evaluation through solution of the system of equations. Even for just a 10

element beam. this process is slow in comparison to the fixed point iteration.

However, as the length of the period of viscoelastic deformation increases, this relative speed relationship reverses. Eventually, the differential formulation begins to generate solutions more rapidly than the integral method. In the example problem described above, this generally occurred approximately between the second and third time constants. The reason for this change is directly related to the computation of the convolution integral of the integral technique. As time increases, the number of terms in the summation increases linearly. This in turn, increases the number of additions which must be performed and therefore linearly increases the time need for each computation. In contrast, the speed of the Runge-Kutta integration routine is virtually independent of time. Thus, the continually increasing computation effort required in the integral technique eventually exceeds that need for the differential technique thereby reversing the relative speed relationship.

V. Conclusions

Based on the results reported herein and elsewhere [12] it is concluded that the differential formulation procedure presented can be employed for the analysis of quasistatic nonlinear one-dimensional viscoelastic problems. This conclusion is based directly on the high level of correlation between results developed using this formulation technique to those obtained with the previously published integral method for solution of such problems. Additionally, it is noted that both of these methods exhibit exceptionally similar accuracy characteristics with regard to the number of elements employed in the approximation. For both, a relatively low number of elements can be used without engendering any significant errors.

Acknowledgement

The research described above has been performed under NASA Grant No. 3-534. The financial support provided by NASA is gratefully acknowledged by the authors. The authors wish to extend their thanks and appreciation to Dr. C. Chamis of the NASA-Lewis Research Center for his support and for the insights into the problem which he provided during our many technical discussions.

References

1. Christensen, R. M., Theory of Viscoelasticity, Introduction Academic Press, New York, 1982.
2. Rabotnov, Y. N., Elements of Hereditary Solid Mechanics Mir Publications, Moscow, USSR, 1980.
3. Schapery, R.A., "Approximate Methods of Transform Inversion for Viscoelastic Stress Analysis," Proceedings of 4th US National Congress on Applied Mechanics, Vol. 2, 1962, pp. 1075-1085.
4. Kraus, H., Creep Analysis, John Wiley & Sons, New York, 1980.
5. Libove, C., "Creep Buckling of Columns," Journal of the Aeronautical Sciences, Vol. 19, No, 7, 1952, pp. 459-467.
6. Zyczkowski, M., "Geomertically Non-linear Buckling of Bars," IUTAM Colloquium on Creep in Structures, Stanford University, CA, Academic Press, New York, 1962, pp. 307-325.
7. Patel, S. A., "Buckling of Columns in the Presence of Creep," The Aeronautical Quarterly, Vol. 7, No. 2, 1956, pp. 25-134.
8. Hoff, N. J., "A Survey of the Theories of Creep Buckling," Proceedings of the 3rd US National Congress of Applied Mechanics, 1958, pp. 29-49.
9. Rogers, T. G. and Lee, E. H.,"On the Finite Deflection of a Viscoelastic Cantilever," Proceedings of the 4th US National Congress on Applied Mechanics, Vol. 2. 1962, pp. 977-987.
10. Stubstad, J. M. and Simitses, G. J., "Bounding Solutions of Geometrically Nonlinear Viscoelastic Problems," AIAA Journal, Vol. 24, No. 11, 1986, pp. 1843-1850.
11. Thurston, G., "Newton's Method Applied to Problems in Nonlinear Mechanics," Journal of Applied Mechanics, Vol. 32, 1965, pp. 383-388.
12. Stubstad, J. M., "Nonlinear Thermoviscoelastic Analysis of Metallic PLane Curved Beams," Doctoral Thesis submitted in partial fulfillment of the requirements for the degree of Doctor of Philosophy, Georgia Institute of Technology, Atlanta, GA, 1986.
13. Vinogradov, A. M., "Nonlinear Effects in Creep Buckling Analysis of Columns," Journal of Engineering Mechanics, Vol. 111, No. 6, 1985, pp. 757-767.
14. Vinogradov, A. M. and Wijeweera, H., "Theoretical and Experimental Studies on Creep Buckling," Proceedings of the 26th AIAA/ASME/ASCE/AHS Structures, Structural Dynamics and Materials Conference, 1985, Vol. 1., pp. 160-164.
15. Tricomi, F. G., Integral Equations, Dover, N.Y., 1985.

NON-ISOTHERMAL ELASTOVISCOPLASTIC SNAP-THROUGH AND CREEP BUCKLING OF SHALLOW ARCHES

G. J. Simitses [1] and R. Riff [2]
School of Aerospace Engineering
Georgia Institute of Technology
Atlanta, Georgia 30332

Abstract

The problem of buckling of shallow arches under transient thermomechanical loads is investigated. The analysis is based on nonlinear geometric and constitutive relations, and is expressed in a rate form. The material constitutive equations are capable of reproducing all non-isothermal, elasto-viscoplastic characteristics. The solution scheme is capable of predicting response which includes pre and postbuckling with creep and plastic effects. The solution procedure is demonstrated through several examples which include both creep and snap-through behavior.

I. Introduction

Elastic snap-through of low arches under quasi-static loads has been the subject of several investigations. The significance of the problem, in so far as it illustrates certain important features in more complicated buckling problems of plates and shells, was pointed out by Marguerre [1], who constructed a simplified mechanical model to demonstrate these features. Timoshenko [2] obtained an approximate solution to the problem of a low arch under a uniformly distributed load. Biezeno [3] considered the problem of a low parabolic arch loaded laterally at the mid-point with a concentrated load. He also investigated snap-through buckling of a shallow spherical cap, pinned along its circular boundary, under the action of a concentrated load applied along the axis of rotational symmetry. He presented his approximate solutions by means of load-deflection curves and equations from which the critical load could be calculated.

In 1952, Fung and Kaplan [4] investigated the problem of low pinned arches of various initial shapes and spatial distributions of the lateral load. Their results show that a very shallow arch snaps-through symmetrically, whereas a higher arch buckles asymmetrically. They also ran a limited number of experimental tests, and their experimental data are in good agreement with their theoretical results. About the same time, Hoff and Bruce [5], in investigating the possibility of snap-through buckling of a low pinned arch with a half-sine-wave initial shape under a half-sine-wave distributed dynamic load (suddenly applied with infinite duration), obtained results for the quasi-static load case which are identical to those obtained by Fung and Kaplan for the same problem.

In 1962, Gjelsvik and Bodner [6] obtained an approximate solution to the problem of a low circular arch with a concentrated load at the mid point of the arch and clamped boundary conditions. They also reported on experimental tests, and there is good agreement between their theoretical predictions and their experimental results. Schreyer and Masur [7] obtained an exact solution to their problem (and for the load case of uniform pressure), and they showed that for the concentrated load case,the arch snaps-through symmetrically regardless of the value of the rise parameter. Masur and Lo [8] presented a general discussion of the behavior of the shallow circular arch regarding buckling, post-buckling and imperfection sensitivity. Snapping of low pinned arches resting on an elastic foundation has been investigated by Simitses [9]. This system exhibits all forms of experimentally observed buckling phenomena (smooth and violent) and of theoretically predicted responses (limit point, bifurcation with stable branching and bifurcation with unstable branching), and it is presented with sufficient detail in Ref. 10. Experimental results have also been reported by Roorda [11].

The effects of inelastic material behavior found their way into the literature since the 1960's. Onat and Shu [12] considered the behavior to be one of rigid-perfectly plastic. Fromciosi, Augusti and Sparacio [13] discussed the collapse of arches under repeated loads with inelastic material behavior. Studies of inelastic snap-through buckling of shallow arches were also reported by Lee and Murphy [14]. In addition Augusti [15] investigated plastic buckling of a model of a three hinged arch in 1968, and a more complete analysis of the same model was provided by Batterman [16] in 1971. Finally, the reader who is interested in the ultimate strength of parabolic steel arches with bracing system is referred to Komatsu [17], who considers inelastic in-plane and out-of-plane instabilities and provides design formula for each case.

The elastic response of arches under sudden (dynamic) application of the external loads has been reported by Hoff and Bruce [5], Hsu [21], [22], and Lock [23]. For a more complete bibliography see Ref. 24.

Creep buckling of shallow arches has been investigated by Huang and Nachbar [18], Krajcinovic [19], and Botros and Bienek [20].

As far as the authors know no work has been reported on the non-isothermal elastovisco-plastic behavior of shallow arches. The purpose of this paper is to demonstrate the effect of highly nonlinear material behavior on the snap through and creep buckling of shallow arches.

[1] Professor, Associate Fellow AIAA, Member ASME
[2] Assistant Professor, Member AIAA

II. Elasto-Thermo-Viscoplastic Constitutive Relations

The prediction of buckling loads and postbuckling behavior of structural components, like shallow arches, made of a realistic metallic material and subjected to non-isothermal thermomechanical loads has increased in importance in recent years.

Under this kind of severe loading conditions, the structural behavior is highly nonlinear due to the combined action of geometrical and physical nonlinearities. On one side, finite deformation in a stressed structure introduces nonlinear geometric effects. On the other side, physical nonlinearities arise even in small strain regimes, whereby inelastic phenomena play a particularly important role. From a theoretical standpoint, nonlinear constitutive equations should be applied only in connection with nonlinear transformation measures (implying both deformation and rotations). However, in almost all of the works in this area [25], the two identified sources of nonlinearities are always separated. The separation yields, at one end of the spectrum, problems of large response, while at the other end, problems of viscous and/or non-isothermal behavior in the presence of small strain.

The classical theories, in which the material response is characterized as a combination of distinct elastic, thermal, time independent inelastic (plastic) and time dependent inelastic (creep) deformation components cannot explain some phenomena, that can be observed in complex thermo-mechanical loading histories. This is particularly true when high-temperature non-isothermal processes must be taken into account. There is a sizeable body of literature [25], [26] on phenomenological constitutive equations for the rate and temperature dependent plastic deformation behavior of metallic materials. However, almost all of these new "unified" theories are based on small strain theories and several suffer from some thermodynamic inconsistencies.

In a previous paper [27], the authors have presented a complete set of constitutive relations for nonisothermal, large strain, elasto-viscoplastic behavior of metals. It was shown there [27] that the metric tensor in the convected (material) coordinate system can be linearly decomposed into elastic and (visco) plastic parts. So a yield function was assumed, which is dependent on the rate of change of stress on the metric, on the temperature and on a set of internal variables. Moreover, a hypoelastic law was chosen to describe the thermo-elastic part of the deformation.

A time and temperature dependent viscoplasticity model was formulated in this convected material system to account for finite strains and rotations. The history and temperature dependence were incorporated through the introduction of internal variables. The choice of these variables, as well as their evolution, was motivated by thermodynamic considerations.

The nonisothermal elasto-viscoplastic deformation process was described completely by "thermodynamic state" equations. Most investigators [25], [26] (in the area of viscoplasticity) employ plastic strains as state variables. The authors' previous study [27] shows that, in general, use of plastic strains as state variables may lead to inconsistencies with regard to thermodynamic considerations. Furthermore, the approach and formulation employed in previous works leads to the condition that all the plastic work is completely dissipated. This, however, is in contradiction with experimental evidence, from which it emerges that part of the plastic work is used for producing residual stresses in the lattice, which, when phenomenologically considered, causes hardening. Both limitations were excluded from this [27] formulation. Accuracy of the formulation was checked on a wide range of examples [28].

The constitutive relation will be rephrased here in some different form. For brevity we compile only some notations and fundamental relations which are used in the formulation of the intended constitutive low. For details, see [27] and [28].

Concerning the formulation of constitutive laws it is advantageous to use a material (co-moving) coordinate system. The transformation from the underformed state (metric g_{ik}) to the deformed state can be represented by the tensor:

$$f^i_k = \overset{\circ}{g}{}^{ir}\, g_{rk} \quad \text{or} \quad (f^{-1})^i_k = g^{ir}\, \overset{\circ}{g}_{rk} \tag{1}$$

The total deformation rate is defined by

$$d^i_k = \frac{1}{2} g^{ir} \dot{g}_{rk} = -\frac{1}{2} g_{ir} \dot{g}^{rk} = \frac{1}{2} (f^{-1})^i_r (\dot{f})^r_k = -\frac{1}{2} (\dot{f}^{-1})^i_r f^r_k \tag{2}$$

here $(\dot{})$ denotes time material derivative. The expression

$$\overset{\nabla}{f}{}^i_k = (\dot{f})^i_k + d^i_k f^r_k - d^r_k f^i_r = sym\{(\dot{f})^i_k\} \tag{3}$$

represents the symmetric part of $(\dot{f})^i_k$ or the covariant derivative with respect to time, also called the convected derivation, which is due to Zaremba and Jaumann.

The total deformation can be decomposed according to

$$f^i_k = \overset{\circ}{g}{}^{im}\, \overset{\bullet}{g}_{mr}\, g_{sk} = \overset{(i)}{f}{}^i_r \overset{(r)}{f}{}^r_k \tag{4}$$

where the superscript $\overset{\bullet}{(\,)}$ relates to a fictitious configuration defined by a fictitious reversible process with frozen internal variables. The decomposition of Eq. (4) leads to an additive decomposition of the deformation rate

$$d^i_k = \overset{(r)}{d}{}^i_k + \overset{(i)}{d}{}^i_k \tag{5}$$

$\overset{(r)}{d}{}^i_k$ is related to the reversible deformations, whereas $\overset{(i)}{d}{}^i_k$ denotes the remaining part of the deformation rate.

For the description of the stress state, we introduce the Kirchoff stress tensor s^i_k, which is connected with the real Cauchy stress tensor σ^i_k, by the relation:

$$s^i_k = \frac{\overset{\circ}{\rho}}{\rho} \sigma^i_k \tag{6}$$

Assuming that the elastic behavior is not affected essentially by inelastic deformations, the following hypoelastic incremental law was chosen [27]

$$\overset{(r)}{d}{}^i_k = \frac{1}{2G} \overset{\nabla}{t}{}^i_k + \{\frac{1}{9K} \dot{s}^r_r + \alpha \dot{T}\} \delta^i_k \tag{7}$$

with

- t^i_k : weighted stress deviator
- G : shear modulus
- K : bulk modulus
- α : coefficient of thermal expansion

The following constitutive relations were established [27] for the inelastic behavior.
yield condition:

$$F = (t^i_k - c\, \overset{\circ}{\rho}\, g\beta^i_k)(t^k_i - c\, \overset{\circ}{\rho}\, g\beta^k_i) - k^2(A,T) = f^2 - k^2 > 0 \tag{8}$$

accompanying equilibrium state:

$$\bar{F} = (\bar{t}^i_k - c\,\mathring{\rho}\,g\beta^i_k)(\bar{t}^k_i - c\,\mathring{\rho}\,g\beta^k_i) - k^2(A,T) = \bar{f}^2 - k^2 = 0 \quad (9)$$

evolution law for inelastic deformations:

$$\overset{(i)}{d}{}^i_k = 2\dot{\lambda}(\bar{t}^i_k - c\,\mathring{\rho}\,g\beta^i_k) \quad (10)$$

with

$$\dot{\lambda} = \frac{1}{4\eta}\left(\sqrt{\frac{(t^i_k - c\,\mathring{\rho}\,g\beta^i_k)(t^k_i - c\,\mathring{\rho}\,g\beta^k_i)}{k^2}} - 1\right) \quad (11)$$

and

$$\bar{t}^i_k = \frac{1}{1+4\eta\dot{\lambda}}(t^i_k - c\,\mathring{\rho}\,g\beta^i_k) + c\,\mathring{\rho}\,g\beta^i_k \quad (12)$$

evolution laws for the internal variables:

$$\dot{A} = \frac{1}{\mathring{\rho}}\bar{t}^i_k\,\overset{(i)}{d}{}^k_i \quad (13)$$

$$\overset{\nabla}{\beta}{}^i_k = \xi\,\overset{(i)}{d}{}^i_k \quad (14)$$

if

$$F = 0 \quad and \quad \frac{\partial F}{\partial s^i_k}\overset{\nabla}{s}{}^i_k + \frac{\partial F}{\partial T}\dot{T} > 0 \quad (15)$$

then

$$d^i_k = \overset{(r)}{d}{}^i_k \quad (16)$$

$$\overset{(i)}{d}{}^i_k = 0 \quad and \quad \overset{\nabla}{d}{}^i_k = 2\ddot{\lambda}(t^i_k - c\,\mathring{\rho}\,g\beta^i_k) \quad (17)$$

with

$$\ddot{\lambda} = \frac{1}{8\eta k^2}\left\{2(t^i_k - c\,\mathring{\rho}\,g\beta^i_k)\,\overset{\nabla}{t}{}^k_i - \frac{\partial k^2}{\partial T}\dot{T}\right\} \quad (18)$$

if

$$F = 0 \quad and \quad \frac{\partial F}{\partial s^i_k}\overset{\nabla}{s}{}^i_k + \frac{\partial F}{\partial T}\dot{T} \le 0 \quad (19)$$

or

$$F < 0 \quad (20)$$

then

$$\begin{aligned} d^i_k &= \overset{(r)}{d}{}^i_k \\ \dot{A} &= 0 \\ \overset{\nabla}{\beta}{}^i_k &= 0 \end{aligned} \quad (21)$$

Within the developed frame the elasto-viscoplastic behavior is governed by the scalar material functions $c(s^i_k, T, A, \beta^i_k)$, $k^2(A,T)$, $g(s^i_k, A, T, \beta^i_k)$, $\xi(A,T,\beta^i_k)$, and $\eta(A,T,\beta^i_k)$. These material functions can be determined from a series of monotonic and cyclic processes with proportional and nonproportional paths at different temperature levels [28].

III. General Formulation and Solution Schemes

The rate form of the constitutive equations suggests that a rate approach be taken toward the entire problem so that flow is viewed as history dependent process rather than an event. For this purpose, a complete true ab-initio rate theory of kinematics and kinetics for continuum and curved thin structures, without any restriction on the magnitude of the transformation was presented in Ref. 28. It is implemented with respect to a body- fixed system of convected coordinates, and it is valid for finite strains and finite rotations. The time dependence and large strain behavior are incorporated through the introduction of the time rates of change of the metric and of the curvature.

The constitutive law may be applied to the conservation of momentum via an appropriate variational principle. The principle of virtual power (or of virtual velocities) reads

$$\int_V \sigma^{ij}\delta v_{j,i}dV - \int_V \rho f^j \delta v_j dV - \int_A \nu T^j \delta v_j dA = 0 \quad (22)$$

where δv_j are the virtual velocities, f^j the body forces per unit mass and νT^j the surface tractions. Total differentiation of Eq. (22) yields,

$$\begin{aligned} &\int_V \left(\frac{d\sigma^{ij}}{dt} + \sigma^{ij}d^k_k - v^i_{,k}\sigma^{kj}\right)\delta v_{j,i}dV - \int_V \rho\frac{df^j}{dt}\delta v_j dV \\ &- \int_A \nu\frac{dT^j}{dt}\delta v_j dA + \int_V \sigma^{ij}\left(\frac{d\delta v_j}{dt}\right)_{,i}dV - \int_V \rho f^j\frac{d\delta v_j}{dt}dV \\ &- \int_A \nu T^j\frac{d\delta v_j}{dt}dA = 0 \end{aligned} \quad (23)$$

At any instant, Eq. (23) must be satisfied. The virtual velocity and its time derivative are then independent. Moreover, the last three terms of Eq. (23) are equivalent to Eq. (22). Hence, the principle of the rate of virtual power may be obtained in its concise form. For further classifications, the total derivative of the stress components will be represented by the Jauman derivative, and the following integrals are defined by

$$I_\epsilon = \int_V \overset{\nabla}{\sigma}{}^{ij}\,\delta v_{j,i}dV \quad (24)$$

$$I_d = \int_V (\sigma^{ij}d^k_k - \sigma^{kj}d^i_k)\delta v_{j,i}dV \quad (25)$$

$$I_r = \int_V \omega^i_k\sigma^{kj}\delta v_{j,i}dV \quad (26)$$

Then, substitution in Eq. (23) yields the final form of the principle of the rate of virtual power,

$$I = I_\epsilon + I_d + I_r = \int_V \rho\frac{df^j}{dt}\delta v_j dV - \int_A \nu\frac{dT^j}{dt}\delta v_j dA \quad (27)$$

The quasi-linear nature of the principle of the rate of virtual power suggests the adoption of an incremental approach to numerical integration with respect to time. The availability of the field formulation provides assurance of the completeness of the incremental equations and allows the use of any convenient procedure for spatial integration over the domain V. In the present instance the choice has been made in favor of a simple first order expansion in time for the construction of incremental solutions from the results of finite element spatial integration of the governing equations.

The procedure employed permits the rates of the field formulation to be interpreted as increments in the numerical solution. This is particularly convenient for the construction of incremental boundary condition histories.

The finite element method for spatial discretization has been well documented (see. e.g. Zienkiewicz [29] or Oden [30]) and will not be detailed here. Restricting attention to a single finite element B_m, the velocity field is approximated by $\tilde{v}_i(x^j)$.

$$v_i(x^j) \sim \tilde{v}_i(x^j) = (\Gamma^{\alpha\beta})^T v^\alpha_i(x^j)V^\beta \qquad \alpha,\beta = 1,\ldots,N \quad (28)$$

In Eq. (28), V^α are generalized nodal velocities, $\Gamma^{\alpha\beta}$ is dependent upon the present nodal coordinates, $v_i^\alpha(x^j)$ is a vector of prescribed functions of (x^j), and N is the number of degrees of freedom associated with the element. The matrix $\Gamma^{\alpha\beta}$ is defined by requiring that evaluation of $\bar{v}_i$ at nodal positions yields V^β.

The algebraic counterpart of Eq. (27) after the finite element discretization is the well-known stiffness expression

$$[K]\{\dot{V}\} = \{\dot{P}\} - \{\dot{F}\} \tag{29}$$

with the tangent stiffness matrix $[K]$, the vector of the incremental velocities $\{\dot{V}\}$, and the vector out-of-balance force rates, external force rates $\{\dot{P}\}$ minus internal force rates $\{\dot{F}\}$. The homogenous case of Eq. (29) indicates either the non-uniqueness of the equilibrium path at a stable or unstable bifurcation point or the unique but unstable situation at a limit point. Hence this criterion may be evaluated by a determinant check or supplementary eigenvalue analysis for the load parameter parallel to the loading process.

Even under the condition of static external loads and slowly growing creep effects, the presence of snap-through buckling makes the inertia effects significant. In dynamic analyses, the applied body forces include inertia forces. Assuming that the mass of the body considered is preserved, the mass matrix can be evaluated prior to the time integration using the initial configuration.

Finite element solution of any boundary-value problem involves the solution of the equilibrium equation (global) together with the constitutive equation (local). Both equations are solved simultaneously in a step by step manner. The incremental form of the global and local equations can be achieved by taking the integration over the incremental time step $\Delta t = t_{j+1} - t_j$. The rectangular rule has been applied to execute the resulting time integration.

Clearly, the numerical solution involves iteration. A simplified version [31] of Riks Wempner constant-arc-length method has been utilized. This iteration procedure which is a generalization of the displacement control method also allows to trace the nonlinear response beyond bifurcation points. In contrast to the conventional Newton-Raphson techniques, the iteration of the method takes place in the velocity and load rate space. The load step of the first solution in each increment is limited by controlling the length ds of the tangent. Either the length is kept constant in each step or it is adapted to the characteristics of the solution. In each step the triangular-sized stiffness matrix has to be checked for negative diagonal terms, indicating that a critical point is reached.

IV. Shallow Circular Clamped Arch

The theory and computational procedures described in the preceding sections have been applied to the creep buckling analysis of a shallow circular clamped arch. The problem of the clamped arch beside being of some practical interest contains a number of similarities to that of the uniformly loaded spherical cap. The trend of results of the arch problem serves as a good indicator to the behavior of the latter.

The shallow circular clamped arch subjected to a single central concentrated load, as shown in Fig. 1, is analyzed. The material chosen for the numerical experimentation is the carbon steel C-45 (DIN 1720) with $E = 10^7$ psi, $\nu = 0.3$ and $\sigma_y = 2.7 \times 10^4$ psi at room temperature. The viscoplastic properties (the scalar material functions) were obtained in Ref. 28.

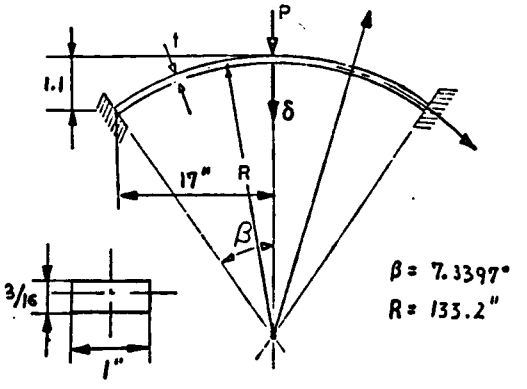

Fig. 1 Clamped Circular Arch

The analysis is performed with the aid of 24 paralinear isoparametric elements, Fig. 2. The paralinear isoparametric element is intended for the analysis of oriented structures where the geometry is such that the thickness is small compared to other dimensions. The characteristics of the element are defined by the geometry and interpolation functions, which are linear in the thickness direction and parabolic in the longitudinal direction (see Fig. 2). Consequently, the element allows for shear strain energy since normals to a mid surface before deformation remain straight, but not necessarily normal to the mid surface after deformation.

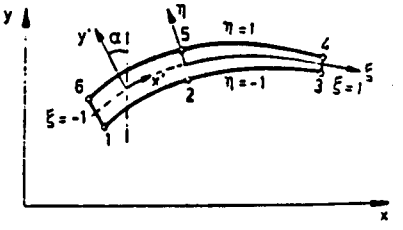

$\xi_o = \xi_i \cdot \xi_i$ $\eta_o = \eta_i \cdot \eta_i$	Node	Ni
	Corner $\xi_i = \pm 1, \eta_i = \pm 1$	$\frac{1}{4}(\xi_o + \xi^2)(1 + \eta_o)$
	Midside $\xi_i = 0, \eta_i = \pm 1$	$\frac{1}{2}(1 - \xi^2)(1 + \eta_o)$

Fig. 2 Paralinear Isoparametric Element

The elastic behavior, corresponding to both axisymetric and asymetric response, is shown on Fig 3. These curves are in complete agreement with those produced by Gjelsvik and Bodner [6], only because the young's modulus and Poisson's ratio values used are virtually the same (carbon steel C-45 here, and

2024-T4 aluminum alloy in Ref. 6). Note that these elastic response curves are hypothetical for our material but true for the 2024-T4 alloy. The true behavior for our material is elasto-viscoplastic and it is labeled as such on Fig. 3. Note that this curve represents quasi-static (steady state) elastovisco- plastic response, as described by the chosen constitutive law. According to this, snapping occurs at a load of 26.20 lbs, primarily because of the low yield strength. Then, the post-limit point behavior seems to be primarily driven by viscoplastic behavior.

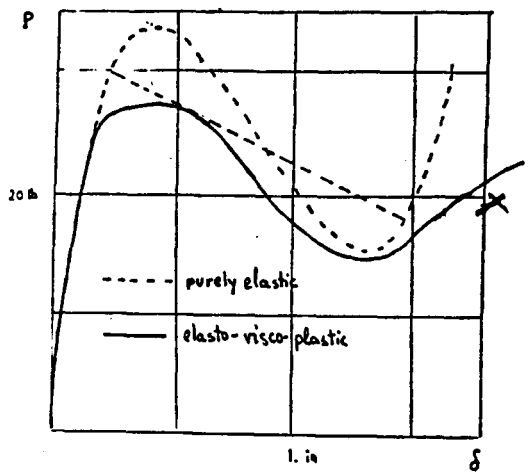

Fig. 3 The Arch Response

It is expected here that if loads up to approximately 14 lbs are reached quasi-statically and left applied for a long time the primary response will be creep and the critical time to creep will be extremely large. On the other hand, for loads between 14 lbs and 26.2 lbs (especially for the higher range) the behavior will be a combination of creep and snap-through buckling. This is best demonstrated by the curve on Fig. 4. The applied load is reached quasi-statically in 13 minutes and then it is kept constant. The curve of Fig. 4 depicts the behavior of the arch in terms of midpoint deflection versus time. Creep, initially, is very slow, then snap-through takes place in 32 minutes, curve BC, and then the creep behavior continues until a critical time to creep (creep buckling occurs) is reached after a total time of 97 minutes. Note that for this loading condition the critical time to creep is 97 minutes. Creep buckling and critical time to creep are based on the phenomenon that the deflection increased very rapidly. For loads higher than 26.2 lbs, it is expected that snapping will occur early, during quasi- static loading and then the creep behavior will be similar to that shown on Fig 4, past point c.

The next example considers the influence of cyclic loading on the response. Figure 5 illustrates the load deflection behavior of the arch under a cyclically applied external load. The load is increased, quasi-statically, from zero to 26 lbs in 5 minutes, then it is held constant for 2.5 minutes, after that it is reduced to 20 lbs and held constant for 50 minutes, then raised to 25.5 lbs for 2.5 minutes and finally it is reduced back to 20 lbs and held constant.

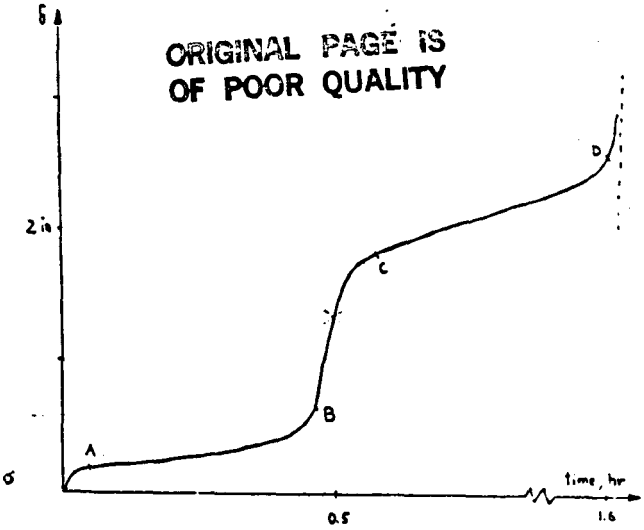

Fig. 4 Deflection Time History

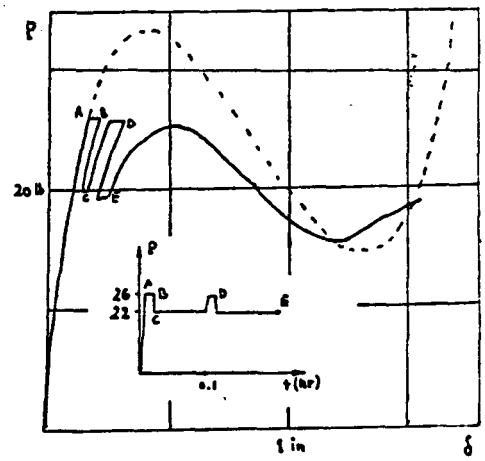

Fig. 5 Multi-Cycle Arch Response

The steady state response under this type of loading exhibits several limit points, which may imply that snapping is imminent shortly after the load reaches the value of 26 lbs (between points A and B on Fig 5). The dashed curve corresponds to the hypothetical elastic static response and it is only shown for comparison purposes.

The last example presented in Fig 6. consider the influence of temperature on the arch behavior. The loading history is the same on the one shown on Fig. 4. The curve corresponding to $T = 50°F$ was discussed previously (Fig. 4), and it is used here as a basis for comparison. When the temperature is raised to $200°F$ (after this, the loading is applied), the time to snap is reduced to 26 minutes, while the critical time to creep is not appreciable affected. On the other hand at the highest temperature $T = 1000°F$, for which results are shown. The critical time to creep is reduced to 62 minutes, and the steady state response does not show a clear snap-through behavior.

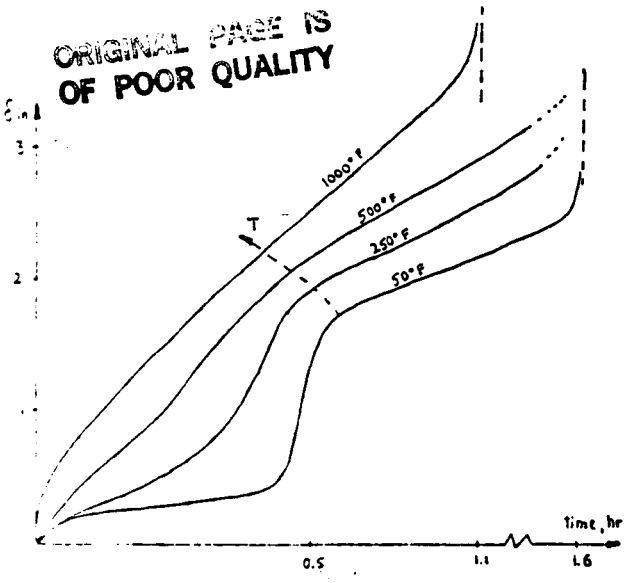

Fig. 6 The Influence of Temperature Raise

V. Discussion

As noted earlier, the main thrust of this work has been to demonstrate the effect of highly nonlinear material behavior on the snap through and creep buckling of shallow arches. It is evident that in the presence of both elastic and viscoplastic deformation the process of buckling assumes an entirely new character. Buckling develops as a time-temperature dependent deformation process under constant or variable loads of magnitudes smaller than the elastic critical values. In arches under loads below the critical values the structure initially deform quasi-statically with the thermo-viscous terms manifesting themselves in the form of increasing displacement under, say a constant load. When the magnitude of the displacements reaches a certain threshold state, the arch snaps dynamically into the post-buckling configuration and then continues quasi-static deformation again.

The material constitutive relation has been proven to be capable of reproducing the main characteristics of viscoplastic deformations. The modified Riks/Wempner iteration scheme has been found to be a versatile technique in the pre-and post critical range.

The influence of thermo-mechanical coupling can become very large in stability problems. Such processes are always connected with a rapid growth of inhomogeneity of the state. Thorough investigation of such problems, however, must be performed with the necessary detail.

Acknowledgement

The research described above has been performed under NASA Grant No. 3-534. The financial support provided by NASA is gratefully acknowledged by the authors. The authors also wish to extend their thanks and appreciation to Dr. C.C. Chamis of the NASA-Lewis Research Center for his support and for the insights into the problem which he provided during our many technical discussions.

References

1. Marrguerre, K., "Die Durchschlagskraft eines Schwach Gekrummten Balken", Sitz. Berlin Math. Gess., Vol 37, 1938, pp 92-108.

2. Timoshenko, S.P., "Buckling of Curved Bars with Small Curvature", J. Appl. Mech., Vol 2, No. 1, 1935, pp 17-23.

3. Biezeno, C.B., "Das Durchschlagen eines Schwach Gekrummten Stabes", Zeitschrift Ange. Math. und Mekh Vol 18, 1938, pp 21-29.

4. Fung, Y.C., and Kaplan, A., "Buckling of Low Arches or Curved Beams of Small Curvature", NACA TN 2840, Washington, D.C., 1952.

5. Hoff, N.J., and Bruce, V.G., "Dynamic Analysis of the Buckling of Laterally Loaded Flat Arches" J. Math. and Phys., Vol 32, No. 4, 1954, pp 276-288.

6. Gjelsvik, A., and Bodner, S.R., "The Energy Criterion and Snap Buckling of Arches", J. Eng. Mech. Div. ASCE, Vol. 88, EM5, 1962, pp 87-108.

7. Schreyer, H.L., and Masur, E.F., "Buckling of Shallow Arches", J. Eng. Mech. Div., ASCE, Vol. 92, EM4, 1966, PP 1-17.

8. Masur, E.F., and Lo, D.L.C., "The Shallow Arch-General Buckling, Post Buckling, and Imperfection Analysis", J. Struct Mech., Vol 1, No 1, 1972, pp 91-107.

9. Simitses, G.J., "Snapping of Low Pinned Arches on an Elastic Foundation" J. Appl. Mech., Vol. 40, No 3., 1973, pp 741-744.

10. Simitses, G.J., Elastic Stability of Structures, Prentice-Hall Inc., Englewood Cliffs, N.J., 1976; second printing R.E. Krieger Publishing Co., Melbourne, F.L., 1986.

11. Roorda, J., "Stability of Structures with Small Imperfections", J. Eng. Mech. Div., ASCE, Vol 91, EM1, 1965, pp 87-108.

12. Onat, E.T., and Shu, L.S., "Finite Deformation of a Rigid Perfectly Plastic Arch", J. Appl. Mech., Vol. 29, No. 3, 1962, pp 549-553.

13. Franciosi, V., Augusti, G., and Sparacio, R., "Collapse of Arches Under Repeated Loading", J. Struct. Div., ASCE, Vol. 90, ST1, 1964, pp 165-179.

14. Lee, L.H.N., and Murphy, L.M., "Inelastic Buckling of Shallow Arches", J. Eng. Mech. Div., Vol. 94, EM1, 1968, pp 225-239.

15. Augusti, G., "Buckling of Inelastic Arches: Simple Model" Meccanica, Vol 3, 1968, pp 102-105.

16. Batterman, S.C., "Plastic Stability of Arches:Re- Consideration of a Model", Israel J. of Techn., Vol. 9, 1971, pp 467-476.

17. Kamatsu, S., "Braced Steel Arches" Ch. 9 in Steel Framed Structures; Stability and Strength, ed. by R. Narayanan, Elsevier Applied science Publishers Ltd, London, 1985.

18. Huang, N.C., and Nachbar, W., "Dynamic Snap-Through of Imperfect Viscoelastic Shallow Arches", TR-AF-AFOSR 1226-67, University of California at LaJolla, March 1967.

19. Krajcinovic, D., "Creep Buckling of a Tied Arch" in Stability of Structures Under Static and Dynamic Loads, published by ASCE, New York, 1977.

20. Botros, F.R., and Bienek, M.P., "Creep Buckling of Structures", Proceedings of the AIAA/ASME/ASCE/AHS 24th SDM Conference (AIAA Paper No. 83-0864), May 1983

21. Hsu, C.S., "On the Dynamic Stability of Elastic Bodies with Prescribed Initial Conditions", Int'l J. Eng. Sci., Vol. 4, 1966, pp 1-21.

22. Hsu, C.S., "The Effects of Various Parameters on the Dynamic Stability of a Shallow Arch", J. Appl. Mech., Vol. 34, No.2, 1967, pp 349-358.

23. Lock, M.H., "The Snapping of a Shallow Sinusoidal Arch Under a Step Pressure Load", AIAA J., Vol. 4, No. 7, 1966, pp 1249-1256.

24. Simitses, G.J., "Suddenly-Loaded Structural Configurations", J. of Eng. Mech., ASCE, Vol. 110, No. 9, 1984, pp 1320-1334.

25. Walker, K.P., "Research and Development Programs for Nonlinear Structural Modeling with Advanced Time Temperature Dependent Constitutive Relations", NASA Contract Report, NASA CR 165533; 1981.

26. Chan, K.S., Bodner, S.R., Walker, K.P., and Lindholm, U.S., "A Survey of Unified Constitutive Theories", NASA Contract Report, NASA-23925, 1984.

27. Riff, R., Carlson, R.L., and Simitses, G.J., "The Thermodynamically Consistent Constitutive Equations For Nonisothermal Large Strain, Elasto-Plastic, Creep Behavior", AIAA/ASME/ASCE/AHS 26th SDM Conf., Orlando, Florida, April 1985, AIAA Paper No. 85-0621-CP, also in AIAA J.

28. Simitses, G.J., Carlson, R.L., and Riff, R., "Formulation of the Nonlinear Analysis of Shell-Like Structures, Subjected to Time-Dependent Mechanical and Thermal Loading" NASA Report, 1986.

29. Zienkiewicz, O.C., and Cheung, Y.K., The Finite Element Method in Structural and Continuum Mechanics, McGraw-Hill, 1967.

30. Oden, J.T., Finite Elements of Nonlinear Continua, McGraw Hill, 1972.

31. Ranum, E., "Strategies for Tracing the Nonlinear Response Near Limit points", Proceedings Europe-U.S. Workshop on "Nonlinear Finite Element Analysis in Structural Mechanics", Bochum, 1980, Springer-Verlay 1981.